How to cite: *Angew. Chem. Int. Ed.* **2023,** *62,* e202217196
International Edition: doi.org/10.1002/anie.202217196
German Edition: doi.org/10.1002/ange.202217196

Water Oxidation Catalysis

Multimodal Analysis of Light-Driven Water Oxidation in Nanoporous Block Copolymer Membranes**

Julian Kund[+], Jan-Hendrik Kruse[+], Andreas Gruber, Ivan Trentin, Marcel Langer, Clarissa Read, Gregor Neusser, Dominik Blaimer, Ulrich Rupp, Carsten Streb, Kerstin Leopold, Felix H. Schacher,* and Christine Kranz**

Abstract: Heterogeneous light-driven catalysis is a cornerstone of sustainable energy conversion. Most catalytic studies focus on bulk analyses of the hydrogen and oxygen evolved, which impede the correlation of matrix heterogeneities, molecular features, and bulk reactivity. Here, we report studies of a heterogenized catalyst/photosensitizer system using a polyoxometalate water oxidation catalyst and a model, molecular photosensitizer that were co-immobilized within a nanoporous block copolymer membrane. Via operando scanning electrochemical microscopy (SECM), light-induced oxygen evolution was determined using sodium peroxodisulfate ($Na_2S_2O_8$) as sacrificial electron acceptor. Ex situ element analyses provided spatially resolved information on the local concentration and distribution of the molecular components. Infrared attenuated total reflection (IR-ATR) studies of the modified membranes showed no degradation of the water oxidation catalyst under the reported light-driven conditions.

Introduction

Heterogeneous catalysis is a cornerstone of modern chemical research, and most industrial chemical processes use one or more heterogeneous catalysts.[1] More recently, the field of sustainable energy has become one of the main drivers of heterogeneous catalyst development, as the splitting of water into hydrogen (H_2) and oxygen (O_2) is one of the major paths to carbon-neutral fuels.[2] One particularly promising approach to this end is artificial photosynthesis where chemical and materials solutions for light-driven water splitting are developed.[3] The concept relies on highly active and stable catalysts for the hydrogen evolution reaction (HER) and water oxidation catalysis (WOC).[4] Specifically, the 4-proton-4-electron WOC is a bottleneck, as suitable catalysts must combine high redox-activity and oxidative/hydrolytic stability with economic viability.[5] This has led to materials design approaches ranging from single-atom catalysts[6] to molecules,[7] clusters,[8] nanoparticles[9] and bulk materials.[5,10] Independent of the type of catalyst, there is common consensus that photo(electro)catalytic water splitting schemes require the use of heterogeneous or heterogenized catalysts to ensure their compatibility with large-scale technological deployments.[11] Thus, high-performance heterogeneous WOCs based on earth-abundant components,[4a,12] embedded in suitable supports are developed. To-date, most heterogeneous or heterogenized WOC relies on bulk reactivity analyses, such as quantification of the evolved O_2 in solution and/or the gas phase using fluorescence-based oxygen sensors,[13] head-space gas chromatography, or Clark-type electrodes.[14] While these approaches provide viable averaged (bulk) information on the performance of the catalyst (i.e. amount of O_2 evolved per gram of catalyst material), no information, e.g., regarding possible heterogeneity of the matrix, or distribution and

[*] J. Kund,[+] A. Gruber, Dr. G. Neusser, D. Blaimer, Prof. Dr. K. Leopold, Prof. Dr. C. Kranz
Ulm University, Institute of Analytical and Bioanalytical Chemistry
Albert-Einstein-Allee 11, 89081 Ulm (Germany)
E-mail: christine.kranz@uni-ulm.de

J.-H. Kruse,[+] Prof. Dr. F. H. Schacher
Friedrich-Schiller University Jena, Institute of Organic Chemistry and Macromolecular Chemistry
Lessingstraße 8, 07743 Jena (Germany)
and
Jena Center for Soft Matter (JCSM)
Philosophenweg 7, 07743 Jena (Germany)
E-mail: felix.schacher@uni-jena.de

Dr. I. Trentin, M. Langer, Prof. Dr. C. Streb
Ulm University, Institute of Inorganic Chemistry
Albert-Einstein-Allee 11, 89081 Ulm (Germany)

M. Langer, Prof. Dr. C. Streb
Johannes Gutenberg University Mainz, Department of Chemistry
Duesbergweg 10–14, 55128 Mainz (Germany)
E-mail: carsten.streb@uni-mainz.de

Dr. C. Read, Dr. U. Rupp
Ulm University, Central Facility of Electron Microscopy
Albert-Einstein-Allee 11, 89081 Ulm (Germany)

[+] These authors contributed equally to this work.

[**] A previous version of this manuscript has been deposited on a preprint server (https://doi.org/10.5281/zenodo.5722330).

molecule-in-matrix stability of catalysts is obtained. Critical insights into the catalytic performance of reactive sites, e.g., photosensitizer molecules or water oxidation sites, are not accessible by bulk methods. In addition, fundamental limitations of the material, e.g., poor light-penetration into the bulk materials, inaccessibility of catalytic sites, inhomogeneous distribution of the active compounds, or major mass-transport limitations cannot be extracted from these bulk measurements. In this regard, we use scanning electrochemical microscopy (SECM) to measure locally the O_2 evolution and correlate the SECM data with micro-X-ray fluorescence spectroscopy (μXRF) and scanning transmission electron microscopy/energy-dispersive X-ray spectroscopy (STEM/EDX) data that reveal the element distribution within the matrix at different length scales. By this approach, we demonstrate how spatially and temporally resolved in situ/operando WOC reactivity data and ex situ information on spatial distribution can be obtained for molecular photosensitizer and molecular WOC systems heterogenized within nanoporous block copolymer membranes. The concept is inspired by studies where SECM has been employed for H_2/O_2 quantification at the surface of photocatalytic systems including $BiVO_4$-based semiconductors,[15] photoanodes,[16] cobaloxime HER catalysts,[17] and manganese-based WOC electrocatalysts.[18]

We use SECM to locally determine the O_2 evolution rate for light-driven heterogenized WOC, using the prototype ruthenium photosensitizer $[Ru(bpy)_3]^{2+}$ (=Ru-PS; bpy=2,2′-bipyridine),[19] which features well-understood photophysics and is characterized by high oxidative redox-potentials capable of driving many WOCs. As WOC, we chose the polyoxometalate (POM) cluster $[Co_4(H_2O)_2(PW_9O_{34})_2]^{10-}$ (=POM-WOC),[20] whose WOC activity under a range of photochemical and electrochemical conditions has been explored. So far, the POM-WOC has been mainly embedded in polymeric membranes for electrocatalytic anodes.[21] Here, we demonstrate the heterogenization of the active components using nanoporous membranes based on polystyrene-*block*-poly(2-(dimethylamino)ethyl methacrylate) (PS-*b*-DMAEMA), where hydrophilic PDMAEMA units can be positively charged by protonation[22] to facilitate POM-WOC immobilization. The hydrophobic polystyrene (PS) block provides a mechanically rigid membrane scaffold (Figure 1a). The light-induced reaction Scheme using $Na_2S_2O_8$ as sacrificial electron acceptor is depicted in Figure 1b.

The resulting PS-*b*-PDMAEMA block copolymers were then used to prepare nanoporous membranes via the so-called NIPS (non-solvent induced phase separation) process.[23] This type of membrane has recently been successfully applied for the heterogenization of POM-based oxidation catalysts for the oxidation of organic compounds like anthracene or tetrahydrothiophene,[24] as well as Ru-PS and thiomolybdate catalysts for light-driven hydrogen evolution.[25] Anchoring of the photoactive components can be achieved through electrostatic[26] or covalent interactions.[27]

To the best of our knowledge, the present study reports the first spatially and temporally operando O_2 measurements of soft matter-embedded molecular photoactive

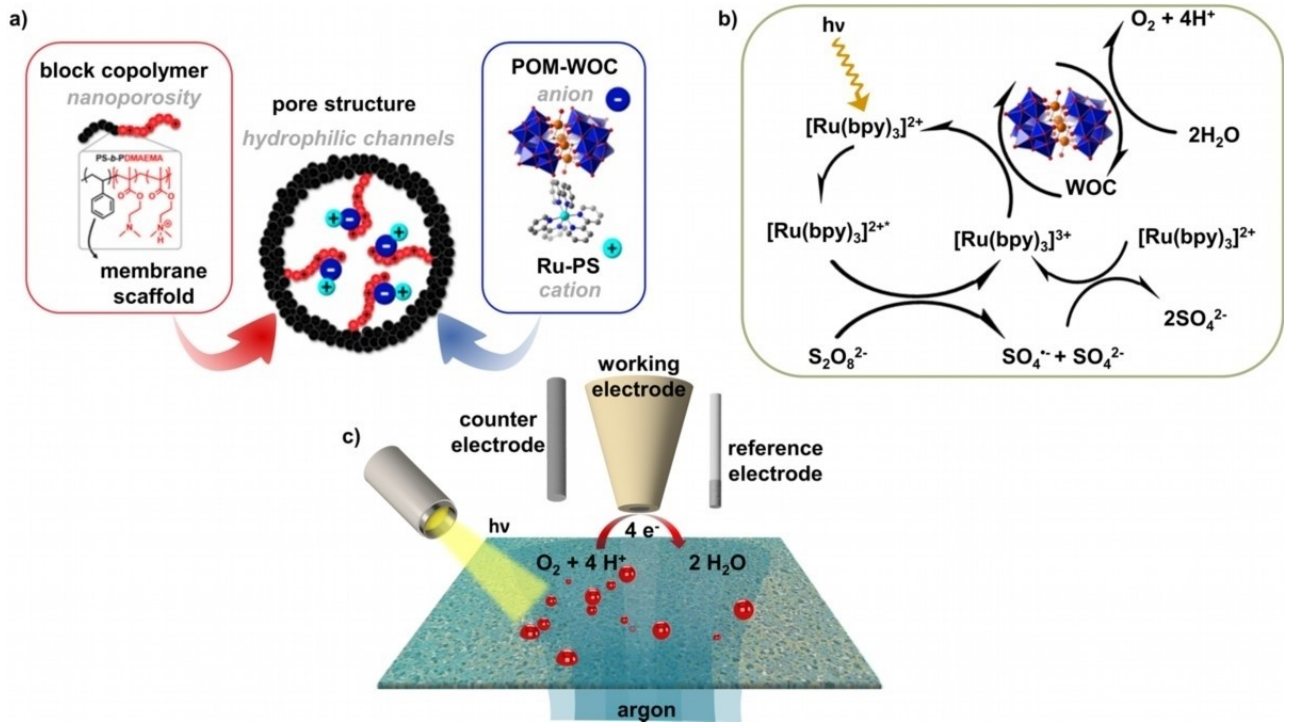

Figure 1. a) Illustration of the nanoporous block copolymer and heterogenized PS and WOC through electrostatic interactions. b) Depiction of the reactions of the light-driven O_2 evolution and c) illustration of local operando O_2 measurements at a nanoporous block copolymer membrane (SEM image in false colours) using SECM.

components, i.e., hereafter referred to as WOCbranes. Conventionally used bulk photocatalytic measurements may result in lower apparent O_2 values, due to O_2 entrapment within the porous nanostructured membrane. SECM enables the time-resolved quantification of dissolved O_2 in close proximity to the membrane surface using a customized SECM setup that allowed gentle purging of the membrane with Argon (Ar) to drive produced O_2 out of the membrane. In combination with ex situ element analysis by STEM/EDX, μXRF, total reflection X-ray fluorescence (TXRF) and high resolution-continuum source-graphite furnace atomic absorption spectrometry (HR-CS-GFAAS), quantitative analysis of Co and Ru could be achieved along with correlated information on homogeneity, morphology and molecular distribution of photosensitizer and catalyst.

Results and Discussion

The Ru-PS and POM-WOC were immobilized in PS-*b*-PDMAEMA block copolymer membranes via electrostatic interactions. In contrast to the reported two-step synthesis procedure of PS-*b*-PDMAEMA by anionic polymerization,[28] we utilized here stepwise nitroxide-mediated polymerization (NMP, Figure S1). In brief, the hydrophobic block was prepared via NMP of styrene forming the membrane scaffold as depicted in Figure S1. In a second step, the PS macroinitiator was used for the NMP of DMAEMA, which led to the final block copolymer PS_{304}-*b*-$PDMAEMA_{71}$ ($M_n = 42{,}900\ g\,mol^{-1}$, $Đ = 1.20$, Figure S2a); the subscripts denote the degree of polymerization in the respective segment. Nuclear magnetic resonance (NMR) measurements (Figure S2b) resulted in a weight fraction of 26–29 wt % of DMAEMA for different WOCbrane batches, which has an increased hydrophilic fraction compared to earlier studies.[22,25,29] Figure S3 shows SEM images of the block copolymer membrane, where the nanoporous nature is clearly visible. The anionic POM-WOC was anchored to the positively charged DMAEMA units by immersion of the membrane into an aqueous POM-WOC-containing solution (see Supporting Information). The anionic POM units (POM-WOC charge: −10) facilitate the subsequent immobilization of the cationic Ru-PS (see Figure 1a and Supporting Information for details). Thermogravimetric analysis gave approximately 38.8 wt% POM-WOC and ca. 3.7 wt% Ru-PS (Figure S2c). Based on earlier results and electrostatic considerations,[25] we assume that the relatively low Ru-PS loading observed is due to repulsive electrostatic interactions between Ru-PS and cationic PDMAEMA chains (Figure 1a).

Scanning electron microscopy (SEM) and transmission electron microscopy (TEM), respectively (see Figure S3 and Figure S4) show the "sponge-like" morphology of the membrane with pores of varying size up to 20–30 μm (blue arrows, Figure S4a, c), and varying shapes and density, which is in line with literature reports for this type of block copolymer membranes.[23a,24,30] The "finger-like" or "rod-like" features with a thickness of ca. 50–60 nm (red arrows, Figure S4b, d) are associated with the block copolymer. The thickness of the membrane can be tuned during fabrication and is typically in the range of approx. 52.5 to 55.4 μm, as determined via SEM and TEM cross-sectional images, however thicker, more rigid membranes up to 100 μm can be obtained. For high-resolution STEM/EDX mapping of the distribution of Ru-PS and POM-WOC within the inner pores of the membrane, the WOCbranes were embedded within an EPON™ epoxy resin.[31] Thereby, artifacts due to sample preparation (e.g., vacuum drying) are avoided (for details see Supporting Information).

The dark fringes adjacent to the rod-like polymeric structures evident in the STEM image (Figure 2) and TEM images (Figure S4) reveal the presence of heavy elements, which originate from the POM-WOC (W and Co) and from the Ru-PS (Ru). These are also clearly discernible in the EDX maps surrounding the rod-like features (i.e., the carbon EDX map shown in Figure S5 reflects the high carbon content of the rod-like polymer structures). The EDX maps show the high oxygen content originating from $[Co_4(H_2O)_2(PW_9O_{34})_2]^{10-}$. The rod-shape and round features visible in the STEM image are related to the orientation of the polymer within the EPON resin and differences in the intensities of the dark fringes are likely related to the orientation as well as sectioning artifacts. The distribution of the mapped elements at the edges of the rod-like structures shows the successful immobilization through electrostatic interactions between positively charged PDMAEMA and the negatively charged POM-WOCs. The element ratio of 0.26 for Co:W derived from the EDX data is in excellent agreement with the element ratio of the POM-WOC itself (Co:W = 0.22). For Ru ($[Ru(bpy)_3]^{2+}$), an unambiguous quantification from EDX data is difficult due to an overlap of the Ru and Cl signals. The difference in energy between Cl (2.62 keV) and Ru (2.58 keV) is only 40 eV. Hence, with a detector resolution of around 130 eV, a clear distinction is impeded.[32] The observed Cl signal (see Figure S5) originates from the $[Ru(bpy)_3]Cl_2$ counter-anions or may originate from residual NaCl used in the POM-WOC crystallization.[20a] Consequently, the Ru content within the modified block copolymer membranes was determined via HR-CS-GFAAS after digestion of small amounts of the WOCbranes. Low Ru concentrations were found, varying among different immobilization batches and storage times of the membranes (see Table S1). A possible explanation for these low concentrations is that the positively charged DMAEMA fraction of the block copolymer partially counteracts the attractive electrostatic interaction of the photosensitizer with the catalyst.

Typically, heterogeneous WOC is predominantly characterized by bulk O_2 detection, which provides no spatially resolved information on the local performance of complex heterogeneous catalysts. Hence, SECM is an attractive alternative for operando O_2 detection, as measurements can be performed in close vicinity to the WOCbranes for determining light-driven WOC activity during illumination. Electrochemical O_2 measurements using microelectrodes have been recently demonstrated to determine photocatalytic WOC activity of the semiconductor strontium titanate ($SrTiO_3$) doped with aluminium,[33] however have not yet

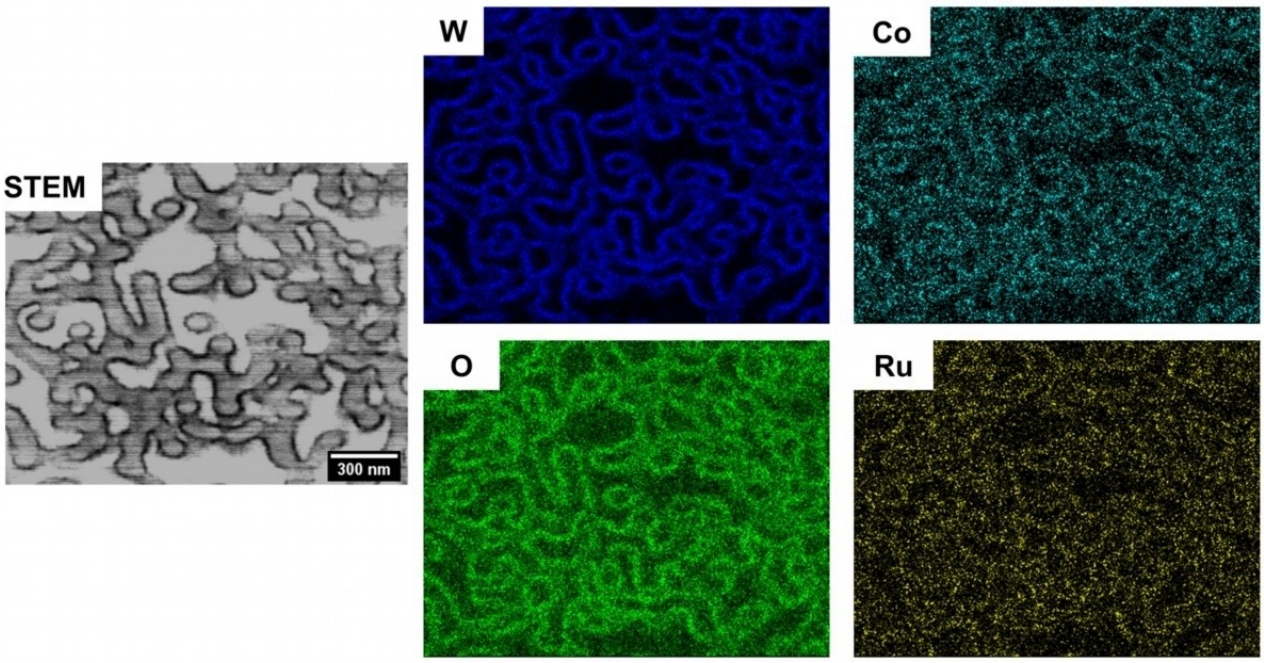

Figure 2. STEM/EDX mapping of the elemental distribution of tungsten (W), cobalt (Co), oxygen (O), and ruthenium (Ru).

been shown for heterogenized molecular water oxidation catalysts. Here, we used static SECM measurements using Pt microelectrodes to quantitatively analyse the light-driven evolution of O_2 (for details on positioning the microelectrode at the membrane, see Figure S6a). A customized SECM cell facilitates illumination of the membrane with a fiber-coupled LED ($\lambda = 470$ nm) and allows simultaneously purging of the membrane with Ar. Current-time (i-t) curves depicting the current response when the membrane is purged either with air (magenta) or Ar (grey) are shown schematically and experimentally in Figure S6b,c. The membranes were purged with Ar (for approx. 15 min) prior to irradiation to remove any O_2 (below the detection limit of our measurements) trapped within the membrane. During the light-driven O_2 measurements, a continuous Ar flow of 1 mL min^{-1} was maintained to drive the produced O_2 out the membrane. Operando O_2 measurements were performed in O_2-free borate buffer solution (pH 8.05) with $Na_2S_2O_8$ as sacrificial electron acceptor[34] in substrate generation/tip collection mode[35] applying a potential of −500 mV vs. Ag/AgCl at the SECM tip.

The pH dependence of the permeability of PDMAEMA membranes has been previously reported.[23a] According to the pore size, O_2 bubbles in the size range around 15 nm should completely pass the membranes at pH 6–10. It has been reported that during homogeneous catalysis, in dependence of the concentrations of the catalyst $[Co_4(H_2O)_2(PW_9O_{34})_2]^{10-}$, the amount of O_2 concentration reached a plateau after 5—15 min of illumination.[36] Three different immobilization batches from two independently synthesized membranes were investigated (in the following termed WOCbrane 1–3). WOCbrane 1 and WOCbrane 2 were illuminated by 60 s intervals separated by 60 s dark intervals. Samples from WOCbrane 3 were constantly illuminated to explore the effect of different irradiation conditions on the photocatalytic performance.[37]

Figure 1c shows schematically the O_2 measurements under irradiation and Figure 3a exemplarily depicts the increase of cathodic current measured at the SECM tip originating from the reduction of O_2 during the individual irradiation steps (chopped illumination, green curve). The same experiments were carried out under dark conditions (magenta curve) and resulted, as expected, in a constant background current.

The current response reveals an initially slow increase in O_2 evolution with a delay of 60 s to 180 s, corresponding to one to three illumination steps, after which an exponential increase of the current with the illumination time is observed for most of the examined WOCbranes (Figure 3b). This behaviour is in contrast to homogeneous photocatalysis of the WOC-POM reported in the literature using the same sacrificial electron acceptor and photosensitizer,[36] although the reported O_2 measurements were obtained via headspace gas chromatography (GC). We hypothesize that the observed delayed onset is mainly attributed to diffusion limitations within the membrane, which is dependent on the actual investigated area. The variation in onset of the O_2 detection for chopped illumination is depicted in Figure 4a. Areas with high polymer density and thus smaller pores may lead to the observed longer delay. It should be noted that the two different WOCbrane 1 and WOCbrane 2 were stored in ultrapure water for different times prior to the SECM measurements and for further ex situ analytical characterization (see Supporting Information).

In addition to the chopped illumination experiments, continuous illumination experiments were carried out for

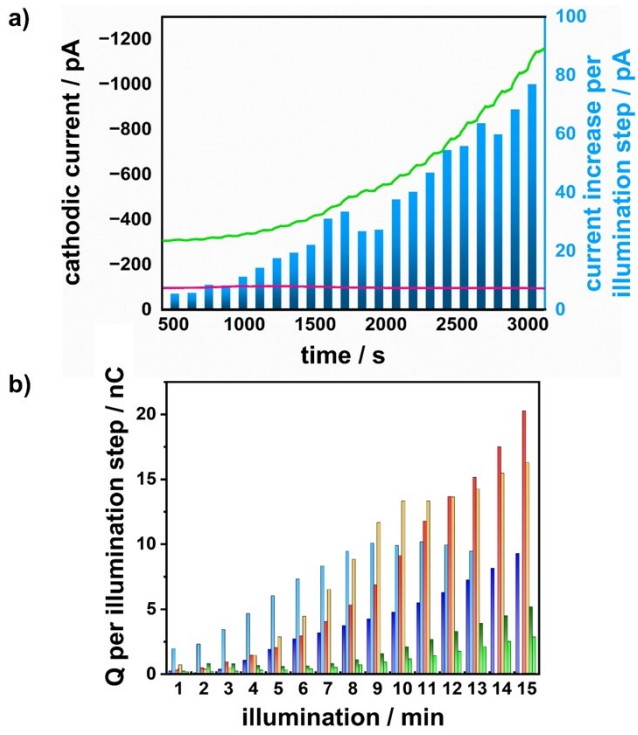

Figure 3. a) Exemplary current response recorded at the microelectrode during illumination (green, illumination was started after 500 s) and under dark conditions (magenta) in 5 mM $Na_2S_2O_8$/100 mM borate buffer solution (see Table S2, measurement membrane 2.2). The cathodic current increase per illumination step is shown by the blue bars. b) Charge evolution during 15 individual irradiation steps (60 s) measured at 6 individual WOCbranes (WOCbrane 1 and 2—two immobilization batches (M1.1 dark blue, M1.2 light blue, M2.1 red, M2.2 orange, M3.1 light green, M3.2 dark green).

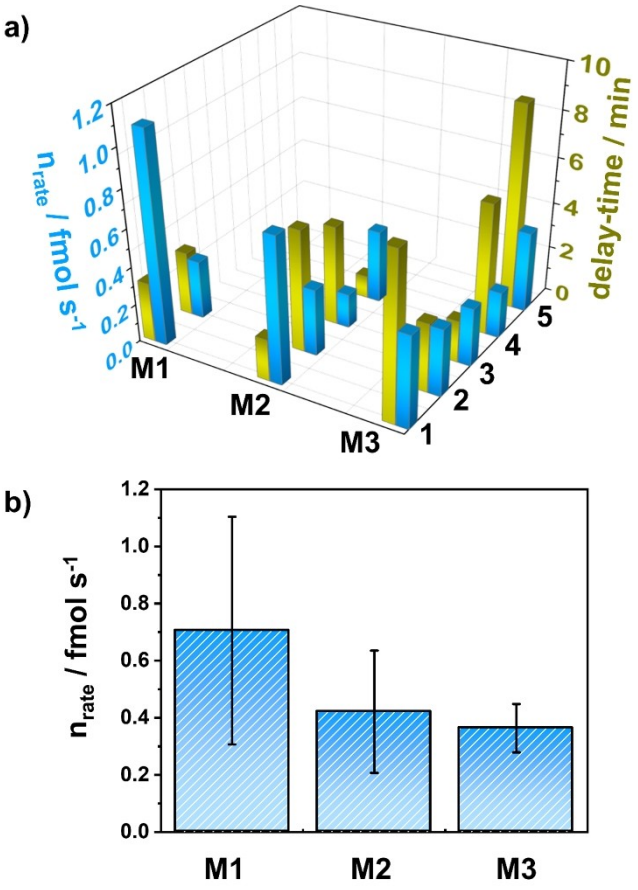

Figure 4. a) Bar diagram showing the reaction rate (blue) and delay time in O_2 evolution (green) for the different membrane batches. b) Amount of O_2 per second (blue bars) of three different immobilization batches from two membranes (M1: $n=2$; M2: $n=4$; M3: $n=6$).

WOCbrane 3 immediately after WOC-POM/Ru-PS loading (i-t curve is shown in Figure S7a**)**. The observed prolonged delay time up to 9 minutes (Figure 4a) observed for WOCbrane 3 may be related to the increased thickness (thickness = 104 µm), which is twice the thickness of WOCbrane 1 and 2. Interestingly, the investigated batches of WOCbrane 3 exhibit a prolonged activity time in the range of 38 minutes up to 66 minutes compared to WOCbrane 1 and 2, where 66 % of the studied patches showed no activity after 15 min of illumination. One sample of WOCbrane 3 was also illuminated under comparable conditions as carried out for WOCbrane 1 and 2 (chopped illumination, Figure S7b). Over a period of 60 illumination steps, this sample exhibits an O_2 evolution-rate of 0.28 fmol s^{-1}, which is in good agreement with the continuously illuminated samples (see Table S2). After storage of the illuminated WOCbranes for several hours in ultrapure water, bubbles of O_2 were observed at the WOCbrane surface as shown in Figure S7c, which may be associated with trapped oxygen.

Figure 4b summarizes the O_2 evolution rate (amount of produced O_2 per second), which was in the range of 0.18 to 1.10 fmol s^{-1} (Table S2) for the different WOCbranes. The apparent variabilities are related to the fact that different areas were probed, which may reflect the heterogeneity in terms of pore space and pore size distribution. Figure S8 shows the change in cathodic current of the three investigated WOCbranes within 15 min illumination, non-modified block copolymer membranes and measurements at the WOCbrane under dark conditions, clearly indicating the photocatalytic activity of the WOCbrane. We performed further studies with respect to the immobilized POM-WOC and Ru-PS content to exclude that this variability in the current response and the time of photocatalytic activity is related to degradation and loss of the WOC. We investigated WOCbranes via EDX prior and after the operando light-driven measurements, as shown in Figure S9. The EDX data show some decrease of W and Co content after illumination which may originate from minor degradation of the WOC or again reflects the heterogeneity of the WOCbrane. Although the same WOCbrane was investigated before and after illumination, the investigated area of the WOCbrane was likely not the same for the EDX measurements. A standard-less quantification of the EDX spectra before and after photocatalytic conditions was used to estimate the ratio between W and Co content. The trend reveals a slight decrease of approximately 4 % in the W signal. This is in line with our TXRF measurements in

leaching experiments, as discussed in the last paragraph and shown in Figure S12.

Degradation of the POM ($[Co_4(H_2O)_2(PW_9O_{34})_2]^{10-}$) was reported for electrochemically driven water oxidation.[38] Thus, to gain insights into POM-WOC stability under the given conditions, the POM-WOC and WOCbranes were spectroscopically investigated before and after illumination. We used infrared attenuated total reflection spectroscopy (IR-ATR) to detect any degradation induced by the immobilization process or photocatalysis. The IR spectra (Figure S10) show the characteristic bands of the pure POM-WOC (blue spectrum) (P–O stretching at 1020 cm^{-1}, W–O stretching at 941 cm^{-1}, W–O–W bending at 872 cm^{-1} and 783 cm^{-1}) and the WOCbrane before (grey spectrum) and after illumination (red spectrum).[20a] Upon immobilization, a shift of the W–O–W bands to higher wavenumbers (from 872 cm^{-1} to 890 cm^{-1} and from 783 cm^{-1} to 795 cm^{-1}, respectively) was observed, which is expected due to the molecular interaction with the block copolymer membrane. More importantly, after illumination, only a small shift of approx. 4–5 cm^{-1} from 795 cm^{-1} to 790 cm^{-1} and 890 cm^{-1} to 886 cm^{-1} of the W–O–W bands was observed indicating no major changes of the molecular structure. Also, no characteristic bands for CoO_x species (e.g., at 510 cm^{-1}, 661 cm^{-1}, 690 cm^{-1}, 840 cm^{-1} and 1013 cm^{-1}) were observed by IR spectroscopy at observable concentrations under the given conditions.[39] Based on this data, we do not observe degradation of the POM-WOC into CoO_x species, either upon immobilization or after 30 min of illumination. This is in line with previous studies, where similar behaviour was reported by Schiwon et al.[40] However, we cannot rule out that small amounts of CoO_x are formed during light-driven catalysis, given the limit of detection (LOD) of our IR-ATR measurements. As expected, also no shift of the characteristic bands of the polystyrene-based block copolymer was observed.

Although, high-resolution STEM/EDX mappings (Figure 2) clearly show a quite uniform presence of POM-WOC, the probed sample sections in these high-resolution maps cover an area of less than 2 μm^2, which is not representative for statistically meaningful evaluation of the macroscopic, homogeneous distribution of WOC and Ru-PS in these molecule-in-matrix systems. This information is crucial for optimization of synthesis and loading procedures of the nanoporous block copolymer membranes to achieve high photocatalytic activity. Moreover, heterogeneities on a larger scale may explain the variations in the observed O_2 evolution, as the probed membrane volume in the SECM experiment is approx. 0.025 mm^3 to 0.05 mm^3 (in dependence of the membrane thickness) giving the overall dimension of the microelectrode (i.e., assuming a cylindrical configuration). As a novel non-destructive 2D elemental mapping method, μXRF remains rarely used for soft materials.[41] However, the technique is ideally suited to study the element distribution of WOC-POM within the membranes on a macroscopic scale, as it gives access to element distribution maps of sample areas up to 20×30 cm, in a concentration range from low ppm up to wt.-%, and with a spatial resolution of about 25 μm. Figure 5 presents exemplary intensity maps of W and Co of WOCbranes from membrane 1 and 3. W and Co were detected in all three investigated WOCbrane batches and evaluation of intensities revealed quite uniform distributions.

To evaluate whether the observed minute variations in the element maps may influence the observed O_2 evolution, the resolution of the electrochemical measurement—providing a probing volume of 0.025–0.05 mm^3 taking the thickness of the membranes into account—was translated to this experiment by summing up of the corresponding μXRF probing volumes. The intensity variation along a marked line (Figure 5a, c) was evaluated by calculation of mean intensities in SECM-analogous probing volumes (Figure 5a,c red squares). As can be seen from the insets in Figure 5a and 5c, the relative intensities differ for Co between 34 and 38 a.u. and for W between 120 and 135 a.u. Intensity variation at blank level (2σ) are 3 a.u. for Co and 5 a.u. for W. Assuming comparable variance in presence of the analyte, these data reveal minor distribution inhomogeneities which may add to the observed variations in O_2 generation. However, most likely other effects, such as inhomogeneity in pore connectivity and/or limitations in diffusion will have a more pronounced effect.

The impact of long-term illumination up to 110 min under photocatalytic conditions was also studied by recording element maps of Co and W in WOCbrane 3. Figure 5b (Co) and 5d (W) show pieces of WOCbrane 3, which were used in SECM experiments and illuminated for 60 min, 110 min, 60 min, and 60 min (left to right) compared to a pristine WOCbrane piece kept in the dark in ultrapure water for storage. Signal intensities for W as well as for Co are on a comparable level for all investigated membrane pieces revealing no significant changes of W and Co load after photocatalysis.

Quantification of Co as catalytically active element, as well as of Ru (photosensitizer) were achieved in digests of WOCbrane pieces via TXRF and HR-CS-GFAAS, respectively. The results are presented in Table S1.

The Co and Ru content of the three investigated replicate samples from WOCbrane 1 and 3 resulted in similar concentrations for Co and Ru, respectively. The found mean Co content for WOCbrane 1 is in the range of 228.0 ± 68.9 to 271.3 ± 65.4 nmol mm^{-3}, whereas as expected, a much lower Ru content of 1.1 ± 0.3 to 1.3 ± 0.4 nmol mm^{-3} was determined (see Table S1). The more rigid WOCbrane 3 (thickness of 104 μm) resulted overall in a lower Co content and a Ru content below the detection limit of 0.1 nmol mm^{-3}, which may be associated with the increased thickness of the membrane. However, the reaction rate is not significantly lower compared to e.g., WOCbrane 2 (M.2.2, see Table S2).

To understand possible effects occurring due to storage, we also studied leaching of Co, W and Ru from WOCbranes 1 and 3 stored in ultrapure water for up to six days. Element contents in the storage solutions were quantified using HR-CS-GFAAS and TXRF, respectively, and were related to the element loss in a membrane volume of 1 mm^3. WOCbrane 1, which had a 3 times higher content of POM and Ru-PS also showed significantly higher leaching com-

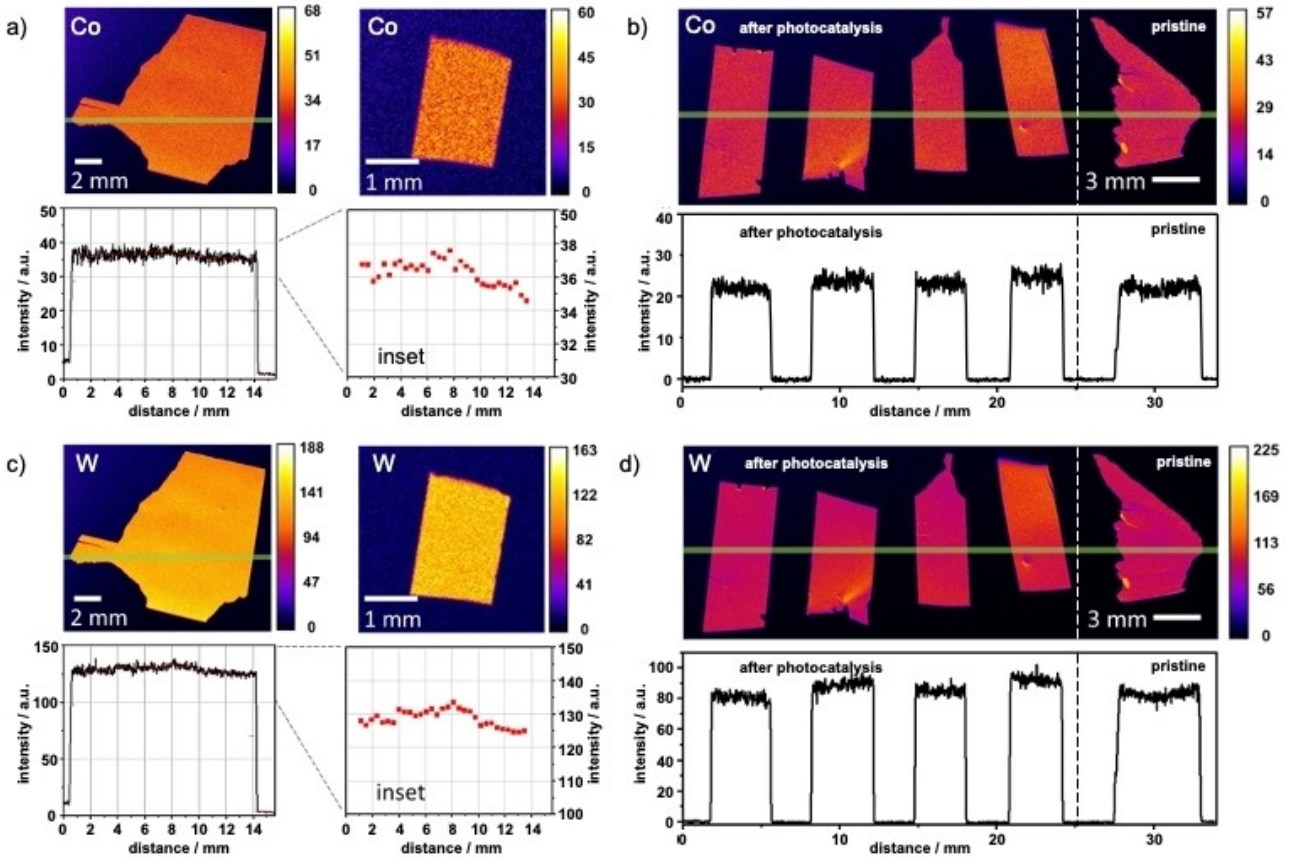

Figure 5. Exemplary element maps (each at the top part) and corresponding intensity distribution along the marked line (each lower part) of cobalt (a, b) and tungsten (c, d) in pieces of WOCbrane 1 (a, c) and WOCbrane 3 (b, d). WOCbrane 1 (a, c) was investigated after preparation and storage in pure water. WOCbrane 3 was investigated either after preparation and storage in pure water (pristine; very right) or after photocatalysis, i.e., immersed in 5 mM $Na_2S_2O_8$/100 mM borate buffer solution and illuminated for 60 min, 110 min, 60 min, and 60 min, respectively. (Resolution in maps and line scans ca. 25 µm; Insets in a, c): red squares are mean values at 400 µm resolution corresponding to SECM probing volume. Line scans in b, d are baseline corrected).

pared to WOCbrane 3 (Figure S11). WOCbrane 3 was investigated directly after immobilization within a period of six days. For the photosensitizer, Ru leaching was observed within the first three days after which the amount of Ru leaching remained constant.

The element ratios of W and Co with ratios between 4.1 and 4.3, as determined by µXRF (WOCbrane 1), fit well with the theoretical value of 4.5. The found molar ratio of Co to Ru of 210 to 219 suggests that only approx. every 50th WOC-POM interacts electrostatically with a photosensitizer molecule, which may be associated with the positively charged PDMAEMA that counteracts the electrostatic interaction of the photosensitizer with the catalyst. Despite the unfavorable ratio of POM-WOC/Ru-PS, and the fact that the heterogenized system suffers from reduced light-penetration of the WOCbrane, as shown in Table S3, the significant light-driven catalytic activity as demonstrated by our SECM measurements, may indicate a favorable, synergistic effect of the molecule-in-matrix system, compensating the relatively low loading of Ru-PS. This is also indicated by the prolonged catalytic activity compared to previous results.[36] It should be noted that for homogeneous photocatalysis in solution typically a significant excess of Ru-PS is used and typical concentration ratios of 0.002–0.01 CAT/Ru-PS are employed.[42]

We also studied possible WOC leaching under photocatalytic conditions that may influence the light-driven activity of the WOCbrane over time. W leaching into the buffer solution was observed under irradiation as well as under dark conditions at a quite low level (see Figure S12) resulting in a maximum W loss of approximately 0.11 pmol mm^{-3} after 120 min. Based on our IR-ATR measurements, we assumed leaching of intact POM with a W to Co atomic ratio of 18 to 4. Thus, Co leaching should be 4.5 times lower than W leaching. In fact, Co concentration in the studied buffer solution was below the limit of detection in all samples. In relation to the initial content of Co in this WOCbrane (89–101 nmol mm^{-3}), we can therefore approximate maximum possible leaching of POM to be in the range of only 0.02 % after 120 min under photocatalytic conditions.

Conclusion

In conclusion, we demonstrated that POM-WOC catalysts and $[Ru(bpy)_3]^{2+}$ photosensitizers can be immobilized within nanoporous block copolymer membranes via electrostatic interactions resulting in active hybrid materials for light-driven water oxidation. Such block copolymer membranes are highly suitable matrices, as the degree of protonation of PDMAEMA and therefore POM-WOC/Ru-PS loadings can be controlled. A thorough characterization of these complex materials based on complementary analysis techniques facilitated obtaining unprecedented insight into the distribution of the WOC-POM and Ru-PS along with quantitative data on membrane loading and photocatalytic activity. SECM is ideally suited for performing spatially resolved, operando measurements of dissolved O_2 at WOCbranes probing sub-millimetre sized areas. Thus, obtained information on variations in O_2 evolution offered insight on the membrane heterogeneity and on possible heterogeneity in WOC-POM/Ru-PS loading, demonstrating that the membrane structure such as distribution of pores may have a significant impact on the observed variations. For high-performance heterogeneous WOCs, the macroscopic uniformity of the CAT/PS distribution is a prerequisite. μXRF element mapping provides access to the homogeneity of WOC elements within the membranes on a macroscopic scale. It was also shown that leaching effects need to be considered during extended storage periods. IR-ATR studies suggest that the immobilized POM stays mainly intact over the duration of the measurements and only small amounts of CoO_x (below the detection limit of our measurements) may be formed. Reduced leaching and prolonged light-driven activity were observed for more rigid (i.e., thicker) membranes, even so these membranes showed lower catalyst loading, which indicates a stabilizing effect by embedding the molecular components into the matrix. We herein present the first successful in situ, local measurements on such heterogenized WOC-POM modified nanoporous block copolymer membranes and to our best knowledge, no bulk measurements of such hybrid materials have been reported so far.

Acknowledgements

The authors acknowledge Prof. Dr. Paul Walther at the Central Facility for Electron Microscopy, Ulm University for his support. The authors thank Riccarda Müller, Ulm University for her assistance with μXRF measurements and data evaluation. The authors acknowledge funding by the German Science Foundation (DFG)—Transregio-SFB—TRR234 "CataLight" (project no: 364549901), projects C4 and B3. Open Access funding enabled and organized by Projekt DEAL.

Conflict of Interest

The authors declare no conflict of interest.

Data Availability Statement

The data that support the findings of this study are available from the corresponding author upon reasonable request.

Keywords: Light-Driven Catalysis · Nanoporous Block Copolymer · SECM · μXRF

[1] R. Schlögl, *Angew. Chem. Int. Ed.* **2015**, *54*, 3465–3520.
[2] a) Q. Wang, K. Domen, *Chem. Rev.* **2020**, *120*, 919–985; b) J. Wang, W. Cui, Q. Liu, Z. Xing, A. M. Asiri, X. Sun, *Adv. Mater.* **2016**, *28*, 215–230.
[3] a) I. Roger, M. A. Shipman, M. D. Symes, *Nat. Chem. Rev.* **2017**, *1*, 0003; b) A. Listorti, J. Durrant, J. Barber, *Nat. Mater.* **2009**, *8*, 929–930; c) T. Faunce, S. Styring, M. R. Wasielewski, G. W. Brudvig, A. W. Rutherford, J. Messinger, A. F. Lee, C. L. Hill, H. DeGroot, M. Fontecave, D. R. MacFarlane, B. Hankamer, D. G. Nocera, D. M. Tiede, H. Dau, W. Hillier, L. Wang, R. Amal, *Energy Environ. Sci.* **2013**, *6*, 1074–1076.
[4] a) P. Du, R. Eisenberg, *Energy Environ. Sci.* **2012**, *5*, 6012–6021; b) Q. Yin, C. L. Hill, *Nat. Chem.* **2018**, *10*, 6–7.
[5] J. Li, C. A. Triana, W. Wan, D. P. Adiyeri Saseendran, Y. Zhao, S. E. Balaghi, S. Heidari, G. R. Patzke, *Chem. Soc. Rev.* **2021**, *50*, 2444–2485.
[6] X.-F. Yang, A. Wang, B. Qiao, J. Li, J. Liu, T. Zhang, *Acc. Chem. Res.* **2013**, *46*, 1740–1748.
[7] S. Berardi, S. Drouet, L. Francàs, C. Gimbert-Suriñach, M. Guttentag, C. Richmond, T. Stoll, A. Llobet, *Chem. Soc. Rev.* **2014**, *43*, 7501–7519.
[8] A. Sartorel, M. Bonchio, S. Campagna, F. Scandola, *Chem. Soc. Rev.* **2013**, *42*, 2262–2280.
[9] S. Ye, C. Ding, M. Liu, A. Wang, Q. Huang, C. Li, *Adv. Mater.* **2019**, *31*, 1902069.
[10] C. Costentin, D. G. Nocera, *Proc. Natl. Acad. Sci. USA* **2017**, *114*, 13380–13384.
[11] S. Jiao, X. Fu, S. Wang, Y. Zhao, *Energy Environ. Sci.* **2021**, *14*, 1722–1770.
[12] B. M. Hunter, H. B. Gray, A. M. Müller, *Chem. Rev.* **2016**, *116*, 14120–14136.
[13] F. L. Huber, S. Amthor, B. Schwarz, B. Mizaikoff, C. Streb, S. Rau, *Sustainable Energy Fuels* **2018**, *2*, 1974–1978.
[14] A. Indra, P. W. Menezes, M. Driess, *C. R. Chim.* **2018**, *21*, 909–915.
[15] H. Ye, H. S. Park, A. J. Bard, *J. Phys. Chem. C* **2011**, *115*, 12464–12470.
[16] a) S. Chen, S. Prins, A. Chen, *ACS Appl. Mater. Interfaces* **2020**, *12*, 18065–18073; b) F. Conzuelo, K. Sliozberg, R. Gutkowski, S. Grützke, M. Nebel, W. Schuhmann, *Anal. Chem.* **2017**, *89*, 1222–1228.
[17] E. Oswald, A. Gaus, J. Kund, M. Küllmer, J. Romer, S. Weizenegger, T. Ullrich, A. K. Mengele, L. Petermann, R. Leiter, P. R. Unwin, U. Kaiser, S. Rau, A. Kahnt, A. Turchanin, M. Delius, C. Kranz, *Chem. Eur. J.* **2021**, *27*, 16896–16903.
[18] Z. Jin, A. J. Bard, *Angew. Chem. Int. Ed.* **2021**, *60*, 794–799.
[19] a) A. W. Adamson, J. N. Demas, *J. Am. Chem. Soc.* **1971**, *93*, 1800–1801; b) V. Balzani, P. Ceroni, A. Credi, M. Venturi, *Coord. Chem. Rev.* **2021**, *433*, 213758.
[20] a) Q. Yin, J. M. Tan, C. Besson, Y. V. Geletii, D. G. Musaev, A. E. Kuznetsov, Z. Luo, K. I. Hardcastle, C. L. Hill, *Science* **2010**, *328*, 342–345; b) N. Li, J. Liu, B. Dong, Y. Lan, *Angew. Chem. Int. Ed.* **2020**, *59*, 20779–20793; c) D. Gao, I. Trentin, L. Schwiedrzik, L. González, C. Streb, *Molecules* **2020**, *25*, 157.

[21] a) S. Herrmann, C. Ritchie, C. Streb, *Dalton Trans.* **2015**, *44*, 7092–7104; b) M. Blasco-Ahicart, J. Soriano-López, J. R. Galán-Mascarós, *ChemElectroChem* **2017**, *4*, 3296–3301.
[22] F. Schacher, T. Rudolph, F. Wieberger, M. Ulbricht, A. H. E. Müller, *ACS Appl. Mater. Interfaces* **2009**, *1*, 1492–1503.
[23] a) F. Schacher, M. Ulbricht, A. H. E. Müller, *Adv. Funct. Mater.* **2009**, *19*, 1040–1045; b) K.-V. Peinemann, V. Abetz, P. F. W. Simon, *Nat. Mater.* **2007**, *6*, 992–996.
[24] I. Romanenko, M. Lechner, F. Wendler, C. Hörenz, C. Streb, F. H. Schacher, *J. Mater. Chem. A* **2017**, *5*, 15789–15796.
[25] I. Romanenko, A. Rajagopal, C. Neumann, A. Turchanin, C. Streb, F. H. Schacher, *J. Mater. Chem. A* **2020**, *8*, 6238–6244.
[26] a) M. Bonchio, M. Carraro, M. Gardan, G. Scorrano, E. Drioli, E. Fontananova, *Top. Catal.* **2006**, *40*, 133–140; b) M. Bonchio, M. Carraro, G. Scorrano, E. Fontananova, E. Drioli, *Adv. Synth. Catal.* **2003**, *345*, 1119–1126.
[27] X. Zhang, P. Tanner, A. Graff, C. G. Palivan, W. Meier, *J. Polym. Sci. Part A* **2012**, *50*, 2293–2318.
[28] W. A. Phillip, R. M. Dorin, J. Werner, E. M. V. Hoek, U. Wiesner, M. Elimelech, *Nano Lett.* **2011**, *11*, 2892–2900.
[29] C. Hörenz, C. Pietsch, A. S. Goldmann, C. Barner-Kowollik, F. H. Schacher, *Adv. Mater. Interfaces* **2015**, *2*, 1500042.
[30] Y. Wang, *Acc. Chem. Res.* **2016**, *49*, 1401–1408.
[31] E. Blaauw, J. Oosterbaan, J. Schakenraad, *Biomaterials* **1989**, *10*, 356–358.
[32] J. J. Friel, *X-Ray and Image Analysis in Electron Microscopy*, 2nd Ed. Princeton Gamma-Tech, **2003**.
[33] T. Kosaka, Y. Teduka, T. Ogura, Y. Zhou, T. Hisatomi, H. Nishiyama, K. Domen, Y. Takahashi, H. Onishi, *ACS Catal.* **2020**, *10*, 13159–13164.
[34] A. L. Kaledin, Z. Huang, Y. V. Geletii, T. Lian, C. L. Hill, D. G. Musaev, *J. Phys. Chem. A* **2010**, *114*, 73–80.
[35] L. Johnson, D. A. Walsh, *J. Electroanal. Chem.* **2012**, *682*, 45–52.
[36] Z. Huang, Z. Luo, Y. V. Geletii, J. W. Vickers, Q. Yin, D. Wu, Y. Hou, Y. Ding, J. Song, D. G. Musaev, C. L. Hill, T. Lian, *J. Am. Chem. Soc.* **2011**, *133*, 2068–2071.
[37] D. Ziegenbalg, A. Pannwitz, S. Rau, B. Dietzek-Ivanšić, C. Streb, *Angew. Chem. Int. Ed.* **2022**, *61*, e202114106.
[38] J. J. Stracke, R. G. Fincke, *J. Am. Chem. Soc.* **2011**, *133*, 14872–14875.
[39] a) M. Zhang, M. de Respinis, H. Frei, *Nat. Chem.* **2014**, *6*, 362–367; b) C.-W. Tang, C.-B. Wang, S.-H. Chien, *Thermochim. Acta* **2008**, *473*, 68–73.
[40] R. Schiwon, K. Klingan, H. Dau, C. Limberg, *Chem. Commun.* **2014**, *50*, 100–102.
[41] a) J.-C. Müller, M. Horstmann, L. Traeger, A. U. Steinbicker, M. Sperling, U. Karst, *J. Trace Elem. Med. Biol.* **2019**, *52*, 166–175; b) A. Mijovilovich, F. Morina, S. N. Bokhari, T. Wolff, H. Küpper, *Plant Methods* **2020**, *16*, 82.
[42] a) B. Schwarz, J. Forster, M. K. Goetz, D. Yücel, C. Berger, T. Jacob, C. Streb, *Angew. Chem. Int. Ed.* **2016**, *55*, 6329–6333; b) J. W. Vickers, H. Lv, J. M. Sumliner, G. Zhu, Z. Luo, D. G. Musaev, Y. V. Geletii, C. L. Hill, *J. Am. Chem. Soc.* **2013**, *135*, 14110–14118.

Manuscript received: November 22, 2022
Accepted manuscript online: March 6, 2023
Version of record online: April 25, 2023